Chapter 2
Zonally Asymmetric Features of the Tropics

2.1 Introduction

This chapter covers the zonally asymmetric climatology of the tropics. Seasonal or monthly mean weather maps are particularly important in the tropics. The following example illustrates this point. Over the North American continent, the January mean sea level isobar map consists of a large continental anticyclone extending southwards from the Arctic and Canada towards the southern United States. This monthly mean pattern does not reveal any of the migrating polar front cyclones that cause much of the weather there during the winter season. The reason for this is that climatological charts in middle latitudes do not display the transient disturbances. A similar exercise carried out over the global tropical belt shows that daily as well as monthly mean charts both carry much the same information. The subtropical highs, the equatorial troughs, the monsoon troughs, the trades of the two hemispheres are common in both the daily and the monthly mean charts. Another way of expressing this is that climatological means carry much of the variance of the total motion field in the tropics. Thus an understanding of the maintenance of the time averaged zonally asymmetric features of the tropics is important.

A detailed description of the time-averaged zonally asymmetric features of the tropics entails knowledge of a number of variables, such as the motion, temperature, pressure and moisture, at a large number of levels in the atmosphere. Much of the information on the time-averaged state of the tropical atmosphere is still not properly documented. Some salient features of the zonal asymmetries of the tropics are presented here.

2.2 Tropospheric Winds at 850 and 200 mb Levels

One of the best sources of reference for time averaged low level flows over the tropics are the reanalysis data sets provided by NCEP and ECMWF. These can provide the mean flow field at 200 and 850 mb levels as shown in Figs. 2.1 and 2.2.
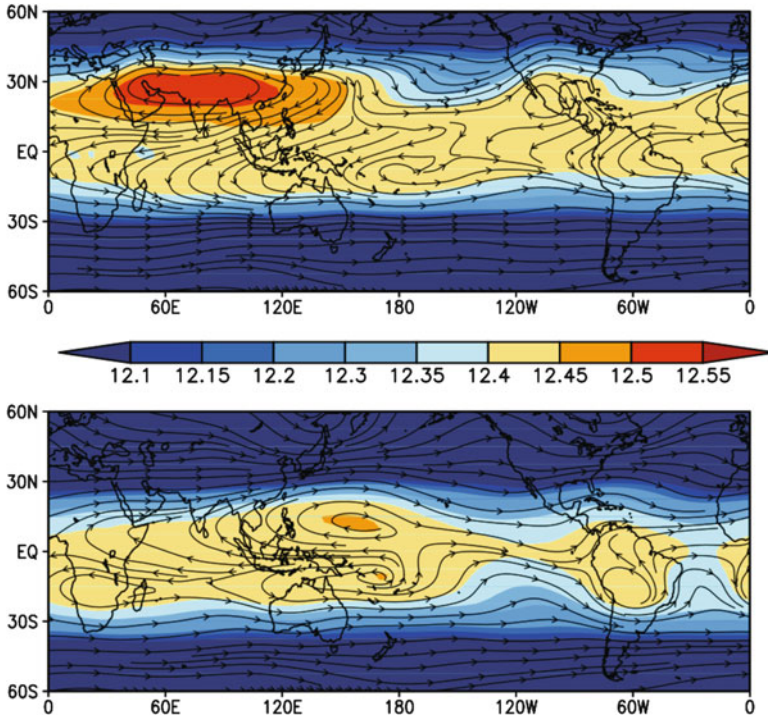
Fig. 2.1 The climatological 200 mb circulation superposed over the corresponding geopotential heights (in km) for boreal summer season (JJA, *top*) and boreal winter season (DJF, *bottom*) (From the NCEP-NCAR reanalysis)

It is clear from these charts that the tropical flows are quite asymmetric in the zonal and meridional directions. The principal asymmetric features at the 200 mb (Fig. 2.1) are:

(i)   The Tibetan anticyclone in JJA;
(ii)   The strong tropical easterlies emanating from the Tibetan high in JJA;
(iii) The Mexican high in JJA over Central America;
(iv)   The pronounced mid-oceanic troughs in the summer hemispheres of the Pacific and Atlantic Oceans;
(v)   The West Pacific high in DJF;
(vi)   The Bolivian high over continental South America in DJF.

Similarly, the principal asymmetric features at the 850 mb (Fig. 2.2) are

(a) The subtropical highs over the oceans;
(b) The tropical convergence zones;
(c) The cross-equatorial monsoon flows of both the summer and winter Asian monsoons;
(d) The heat lows over the deserts;
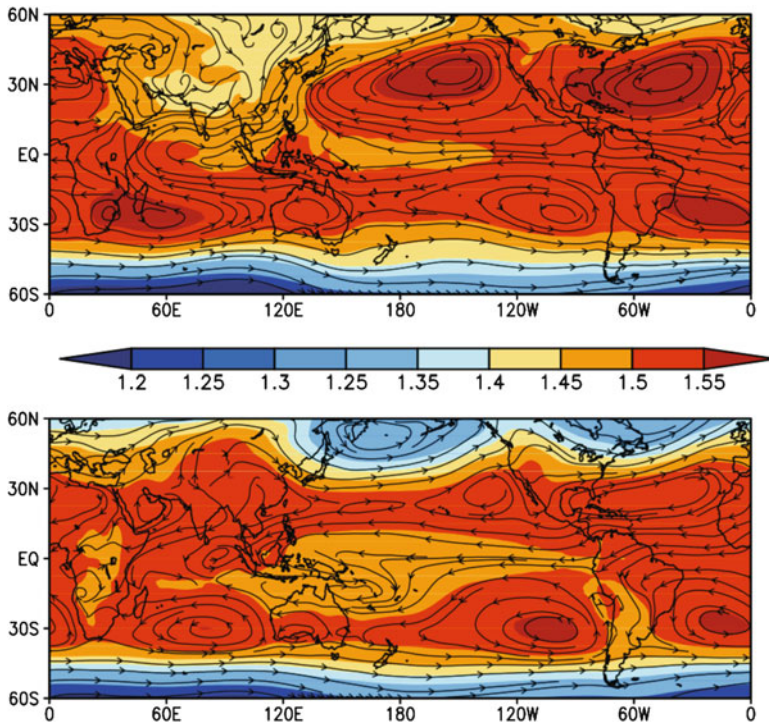(e) The Somali Jet along east Africa.

Fig. 2.2 The climatological 850 mb circulation superposed over the corresponding geopotential heights (in km) for boreal summer season (JJA, *top*) and boreal winter season (DJF, *bottom*) (From the NCEP-NCAR reanalysis)

In Fig. 2.2 the reversal of winds in the lower troposphere from southwesterly to northeasterly between summer and winter monsoonal flows is apparent. The upper troposphere carries a monsoonal upper anticyclone complex that proceeds north from the general region of southern Indonesia and northeastern Australia (in January) to the eastern foothills of the Himalayas (by June). By its nature this anticyclone is a thermal high. Below this traversing high resides the low-level monsoon convection and associated heavy rain. The monsoon rain along the upper anticyclone path can be as large as 200 in. per month. The tropospheric averaged temperatures over this region are warmer than the surroundings due to the large latent heat release of the precipitating systems. The northward propagating anticyclone of the upper troposphere temporarily loses its identity as it approaches and traverses across the equatorial latitudes. At these very low latitudes the monsoon convection cannot sustain an upper level high because of the very low value of the Coriolis force. As a result, what we see at these latitudes is a radial outflow above the rain areas.

The 200 mb monthly mean climatology exhibits one other notable feature, namely, the largest clockwise flow system of the global northern winter climatology. This is the West Pacific high that is located south of Japan. The axis of this high

is oriented from west-northwest towards east-southeast. The lower extremity of this axis extends into the southern hemisphere over the eastern Pacific. This climatological clockwise flow entity spans almost the entire length of the Pacific Ocean. An interesting aspect of this high is that this clockwise flow carries an anticyclone (i.e., high pressure) over the western Pacific Ocean. The same axis, as it crosses the equator over the eastern Pacific Ocean, still carries clockwise flows, but here they are associated with low pressure. Although the winds do not change their polarity (they remain clockwise), the pressure does change polarity (between high and low) as it crosses the equator. This largest climatological system of the tropics deserves further studies. All of these features exhibit seasonal changes.

2.3   The Motion Field in the Upper Troposphere

The mean motion field at 200 mb has received far more attention in recent years because of the availability of high level cloud motion vectors and commercial aircraft wind reports.

   Figures 2.3 and 2.4 illustrate two typical winter and summer maps respectively over the global tropical belt. The salient features of the winter season (Krishnamurti 1961; Sadler 1965) are summarized as follows. The subtropical westerly jet stream
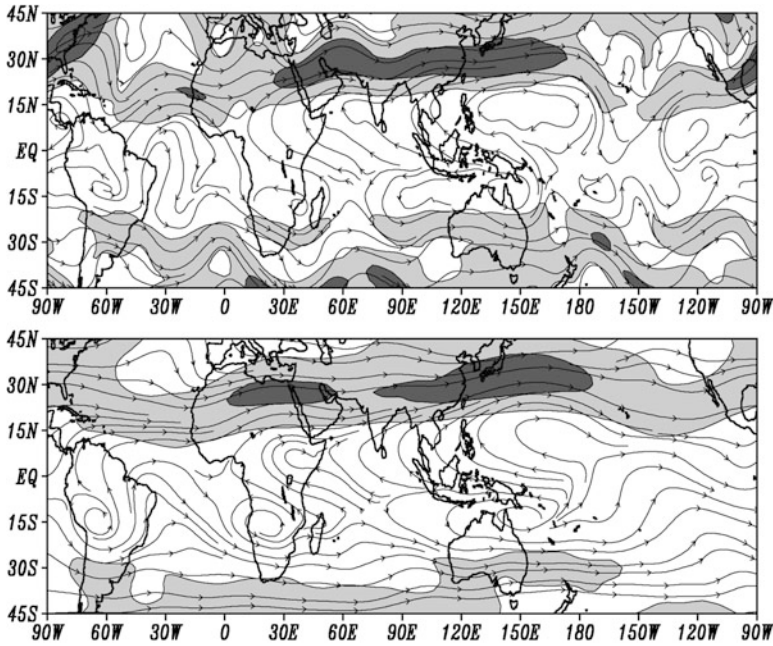

Fig. 2.3 An example of northern winter 200 mb daily (*top*) and seasonal (*bottom*) streamlines and isotachs. The shading interval is 25 m s^{-1} (Computed from the NCEP-NCAR reanalysis)

Fig. 2.4 An example of northern summer 200 mb daily (*top*) and seasonal (*bottom*) streamlines and isotachs. The shading interval is 25 m s^{-1} (Computed from the NCEP-NCAR reanalysis)
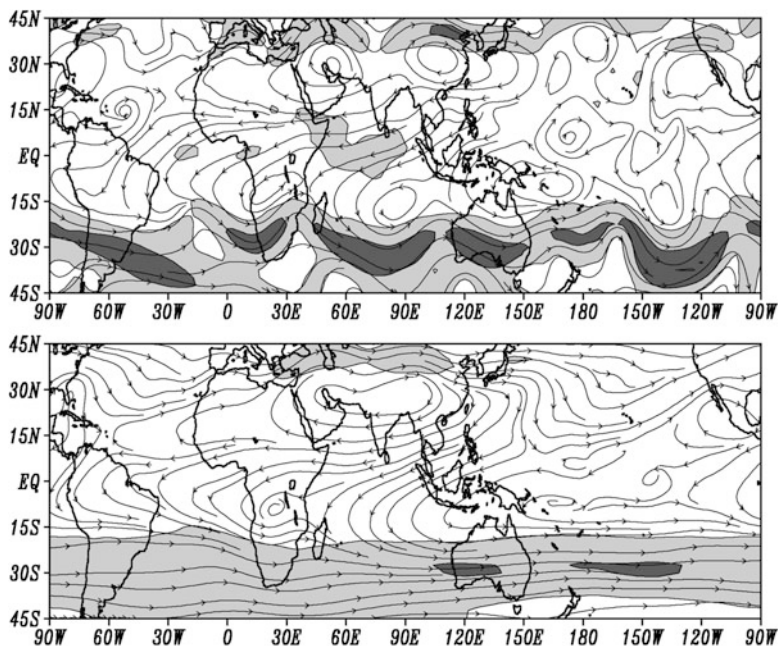
exhibits a quasi-stationary three-wave pattern with maximum velocity off the southeastern United States, the Mediterranean Sea and the coast of Japan. The strongest winds are found in the latter region. The quasi-stationary geometry of the wind-speed field is an unexplained phenomenon. Although there is some evidence of its relation to intense convection over three continental regions of the equatorial tropics, i.e. the northwestern part of South America, central Africa and the Indonesia/Borneo area, these relationships have not been adequately explored.

The latitude of the subtropical jet streams during the northern winter is roughly 27°N (Krishnamurti 1961). During this period the flows over the southern tropical oceans, at 200 mb, exhibit mid-oceanic troughs in the motion field. These quasi-stationary troughs are found in the middle of the Atlantic and in the Indian and the Pacific Oceans (Krishnamurti et al. 1973). Their analogous counterparts are found over the northern tropical oceans during the northern summer, see Fig. 2.4.

The zonal asymmetry of the 200 mb flows during the northern summer has been discussed at some length in the literature (Krishnamurti 1971a, 1971b; Krishnamurti et al. 1973, 1974). The salient climatological features of these flows are: The Tibetan and West African high pressure areas, the mid-Pacific trough, the mid-Atlantic trough, the tropical easterly jet over Asia and equatorial Africa, and the Mexican high. The zonal expanse of the Tibetan High Complex is noteworthy. In the mean it extends for roughly 30W to 150E longitudes. The transients often occupy a larger size.

These large amplitude features of the time-averaged motion field carry about 50 % of the total variance of the total horizontal motion field. Thus one would see most of the above-mentioned features on daily upper-level maps during the northern summer (Krishnamurti et al. 1970, 1975). As stated earlier, it is important to appreciate and obtain a good understanding of the time-averaged large scale zonal asymmetry of the flows.

2.4 The Temperature Field

The most conspicuous aspect of the thermal field is the zonal asymmetry evidently related to the land-ocean distributions. Over the summer hemisphere the air over the land areas is generally warmer than that over the oceanic tropics, the converse being the case over the winter hemisphere. The most pronounced zonal asymmetry is found near the Earth's surface and near the 300 mb surface.

In the boreal summer season, the continental Asian monsoon releases a tremendous amount of latent heating from deep convection over a large fraction of the area. There is also associated subsidence warming in the adjacent Arabian and West African deserts (Rodwell and Hoskins 2001). Figure 2.5 illustrates the point of this zonal asymmetry from the climatological temperature distribution at 300 mb for boreal summer and winter seasons. The former is related to the sensible heat flux from the land areas and the latter to deep convective and subsidence warming.
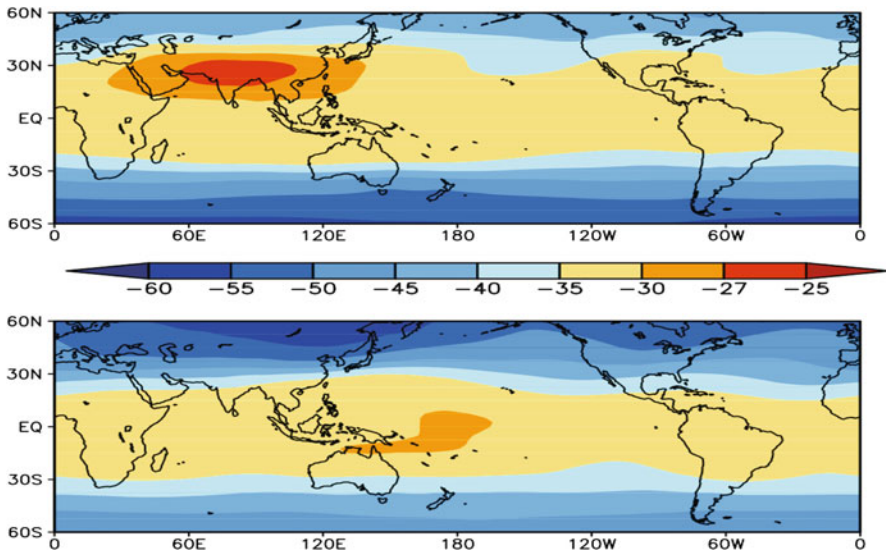

Fig. 2.5 Climatological mean temperature at 300 mb for northern hemisphere summer (JJA, *top*) and northern hemisphere winter (DJF, *bottom*) (From NCEP-NCAR reanalysis. Units of °C)
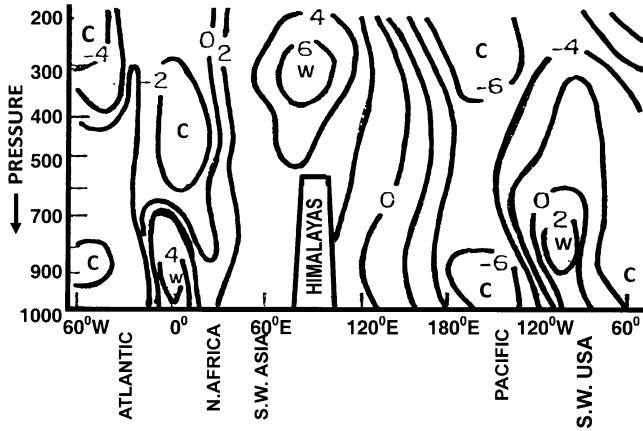
Fig. 2.6 The vertical structure of the temperature anomaly field in boreal summer season at 32°N (After Flohn 1968)

The most pronounced zonal asymmetry occurs during the northern summer (Fig. 2.5, top). In addition to the latent heat release from deep convection, sensible heat from the elevated heat source of the Tibetan plateau is also contributing to this zonal contrast. The highest temperatures are found over the Tibetan Plateau. The mid-oceanic troughs are comparatively cold (Fig. 2.5 top). During the northern winter, the 300 mb zonal temperature gradient is relatively weaker (Fig. 2.5 bottom).

The absence in the southern hemisphere of a vast region of high altitude land mass like the Tibetan plateau, and the relatively smaller spatial extent and consequent reduced release of deep convective heating from the northern Australian and the maritime monsoons are some of the contributing factors for a weaker zonal asymmetry at 300 mb in the boreal winter. During this period the middle oceanic troughs (Fig. 2.5, bottom) over the southern oceans are colder and the anticyclonic circulations near the land areas of the southern hemisphere are relatively warm.

An interesting illustration of the zonal asymmetry of the thermal field comes from Flohn (1968). Figure 2.6 shows a vertical structure of the temperature anomaly field at 32°N where the zonal average is removed from the temperature distribution at each pressure level. The high temperature region over the Tibetan Plateau and relatively colder regions over the oceanic tropics are clearly evident. These time-averaged zonal asymmetries should be viewed along with the geometry of the divergent east–west circulation (presented in the next section) since they have important dynamical implications.

In contrast to the upper air temperatures, the surface air temperatures show a much larger zonal asymmetry between land and ocean in the boreal winter than in boreal summer (Fig. 2.7). This is because of the pronounced radiative heat loss from land and higher heat capacity of the oceans that result in smaller seasonal changes of the ocean temperatures. During the boreal summer season the Asian monsoon rains cool the land-surface thereby reducing the zonal temperature contrast between ocean and land.
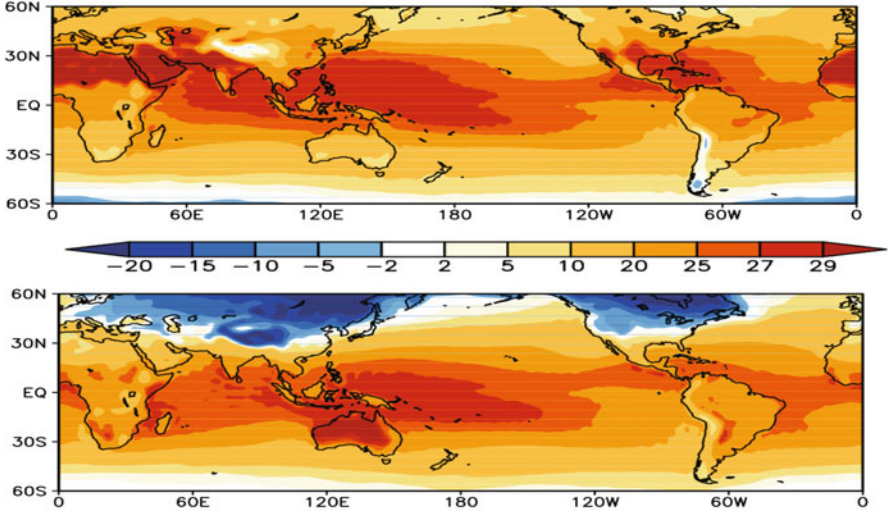
Fig. 2.7 The climatological mean surface air temperature for northern hemisphere summer (JJA, *top*) and northern hemisphere winter (DJF, *bottom*) (From NCEP-NCAR reanalysis)

2.5   The East/West Circulations in the Tropics

The time-averaged east/west circulations are essentially divergent motions and are quite analogous to the Hadley type vertical overturnings described in Chap. 1. Here we decompose a horizontal velocity vector $\mathbf{V}$ into a rotational part, $\mathbf{V}_\psi$, and a divergent part, $\mathbf{V}_\chi$, i.e.,

$$\mathbf{V} = \mathbf{V}_\psi + \mathbf{V}_\chi. \tag{2.1}$$

A time mean velocity potential $\bar{\chi}$ is defined by

$$\overline{\mathbf{V}}_\chi = \nabla \bar{\chi} \tag{2.2}$$

We define the intensity of the Hadley and east/west circulations by the respective relations:

$$I_H = \frac{1}{2\pi} \int_0^{2\pi} \frac{\partial \bar{\chi}}{\partial \varphi} d\lambda \tag{2.3}$$

$$I_E = \frac{1}{\varphi_2 - \varphi_1} \int_{\phi_1}^{\varphi_2} \frac{\partial \bar{\chi}}{\partial \lambda} d\varphi, \tag{2.4}$$

where φ_1 and φ_2 are the southern and northern limits of a tropical channel of interest. Note that I_H varies along φ (latitude), while I_E varies along λ (longitude). A proper geometrical depiction of the Hadley cell can be presented on a meridional vertical plane while that for the east/west circulation would be a zonal plane. The velocity potential for a seasonal mean is obtained as a solution of the equation

$$\nabla^2 \bar{\chi} = \nabla \cdot \overline{\mathbf{V}}, \tag{2.5}$$

where $\overline{\mathbf{V}}$ is a seasonal mean horizontal velocity vector and is assumed to be known. In this discussion there are no east/west boundaries as the latitude band of interest encompasses the globe, and $\bar{\chi}$ is set to zero at the north and south boundaries.

It is important to recognize that most of the variance (about 80 %) of the motion field in the tropics is described by the rotational part (Krishnamurti 1971a). However all circulations in the vertical planes, such as the Hadley and east/west type circulations, are divergent circulations and are not explicitly described by the rotational part of the wind. These divergent circulations are extremely important for the understanding of the time-averaged motion field of the tropics.

The geometry of the climatological velocity potential $\bar{\chi}$ and the corresponding divergent motion field is illustrated in Fig. 2.8 for the boreal summer and winter seasons. The velocity potential isopleths are shaded in blue for the outflow center and in red for the inflow center. Arrows indicate the divergent winds. It is quite clear from Fig. 2.8 that the divergent circulations are present in the zonal as well as the meridional planes. The major center of the east/west circulations during the northern summer season (Fig. 2.8 top) is found on the northern part of the Bay of Bengal, southeast Asia and south China Sea. During the northern winter season, this center of upper level outflow shifts towards Indonesia-Borneo. The streamlines of the divergent part of the flows converge to the mid-oceanic troughs in the summer and winter seasons. During the northern summer the other region of divergent outflow is the Pacific coast of southern Mexico. In the northern winter season, besides the region over Indonesia, the northwestern part of South America, and central Africa also exhibit upper level outflow. These three regions of high-level divergent outflow coincide roughly with the three intense rainfall belts of the northern winter. This geometry may have some important bearing on the wave number three in the quasi-stationary subtropical jet stream of winter discussed earlier.

2.6   The Moisture Field

This is by far the most important scalar field in the tropics. The distribution of the moisture, although to a large extent dynamically controlled, still determines the evolution of many smaller scale disturbances. The presence of desert and oceanic areas makes this field zonally asymmetric. The climatology of the moisture field is very important for the general circulation of the atmosphere. Scientists have asked
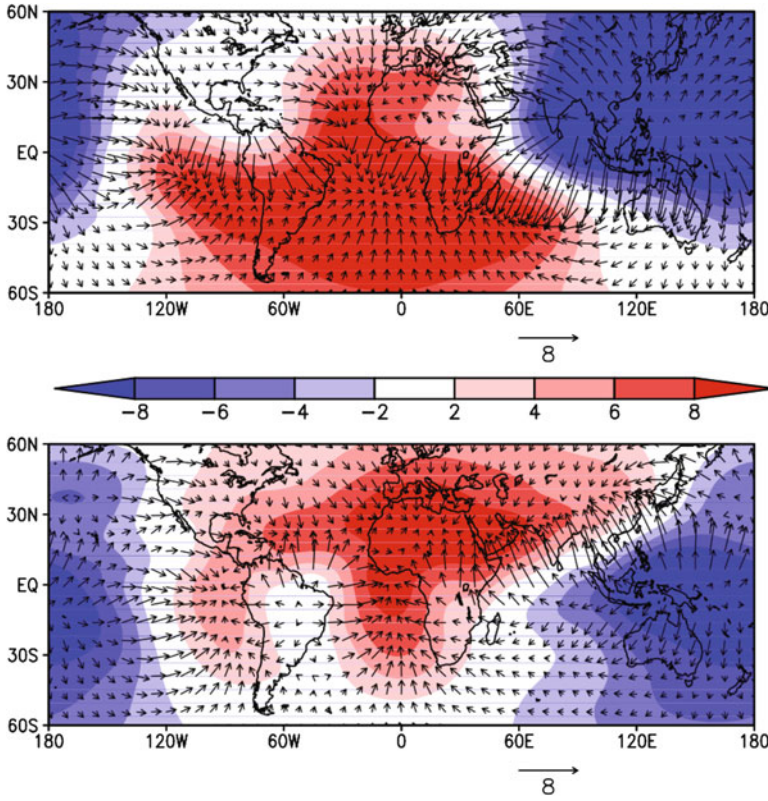
Fig. 2.8 The climatological mean 200 hPa velocity potential (10^6 m^{2}s^{-1}) and divergent wind (ms^{-1}) for JJA (*top*) and DJF (*bottom*) (From the NCEP-NCAR reanalysis). The sample vector represents a divergent wind with magnitude of 8 ms^{-1}

how important the definition of the detailed moisture field is. Some feel that a simple zonally symmetric geometry of the moisture field would adjust to a reasonable geometry in a matter of a few days of numerical integration in global general circulation models. This was, in fact, demonstrated by Mintz in some early runs with a two-level general circulation model. It seems from these studies that the spatial distribution of the time-averaged planetary scale moisture distribution can be explained from simple formulations of sources and sinks and a reasonable simulation of the advection. However, the assumption that the moisture variable is passive and its details somewhat dynamically redundant could be a disastrous one for studying the short-range evolution of tropical weather systems. It is felt that the climatology of the global moisture is an important topic and hence we present here, in Fig. 2.9, the moisture fields for July and January at 850 mb, i.e. the isopleths of specific humidity (g kg^{-1} units).

During the northern winter, three regions of large specific humidity (12 g kg^{-1}) – over the northwestern part of South America, equatorial Africa and over
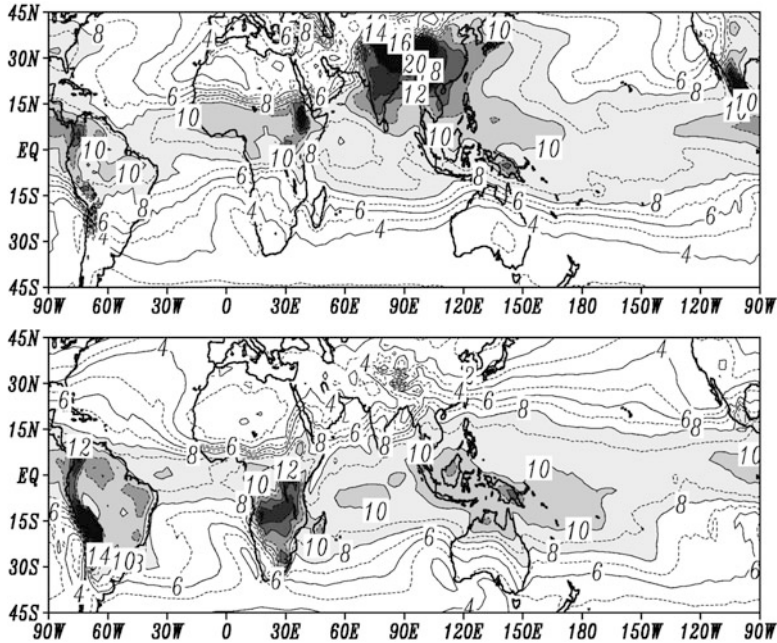
Fig. 2.9 Mean July (*top*) and January (*bottom*) specific humidity. Units are g kg^{-1}, contour interval 1 g kg^{-1} (Computed from NCEP-NCAR reanalysis)

Indonesia – may be noted. These regions were earlier emphasized in the discussion of the northern winter east/west circulation and tropical rainfall belts. During the northern summer the regions of high moisture are found over the monsoon belts near the foothills of the Himalayas (14 g kg^{-1}) and over the equatorial eastern Pacific, again closely related to the location of the divergent outflows shown in Fig. 2.8. Large zonal asymmetries of the moisture field are found during the northern summer near 20°N. Because of the dynamical influences of the motion systems, the specific humidity distribution over the tropical oceans is not uniform. Gradients in the east/west and north/south directions over the oceans are primarily associated with weather systems with ascending and descending motions. The seasonal changes in the distribution of specific humidity are large. The largest values of specific humidity are found over the land areas and not over the oceanic tropics. This is related to larger temperatures of land areas that can hold large amounts of moisture prior to saturation, which makes the monsoon belts very moist.

2.7   The Sea Level Pressure Field

Here we shall present sea-level isobars for January and July (Fig. 2.10). The January features are dominated by the strong pressure gradient near 100°W over Asia, i.e. south of the Siberian surface anticyclone. The subtropical highs are better
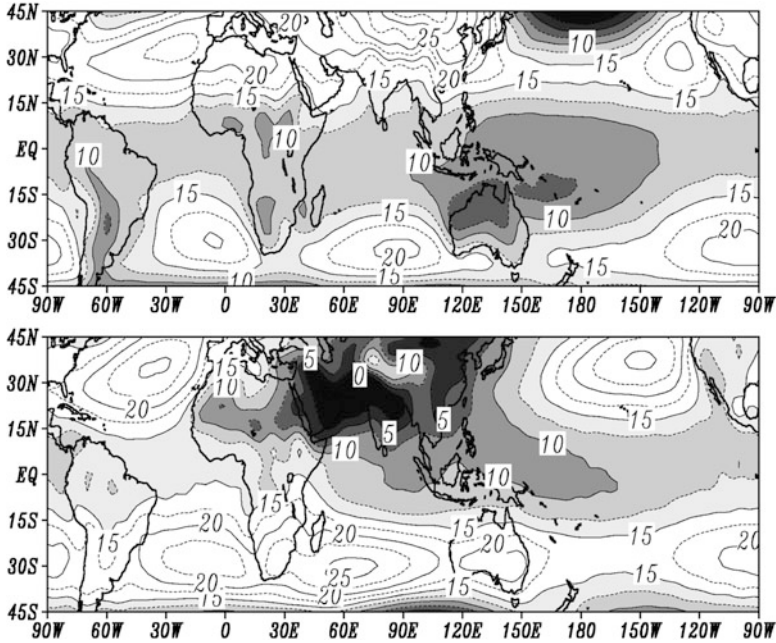
Fig. 2.10 Mean January (*top*) and July (*bottom*) sea level pressure. Units are in mb, contour interval 2.5 mb (Computed from NCEP-NCAR reanalysis)

organized over the northern oceans during the northern summer and less so during the northern winter. The descending branch of the Hadley Cell is more intense near 30°N during northern winter compared to the northern summer (Fig. 2.10). The subtropical highs have intense descending motion towards the eastern part of the anticyclonic circulations. The descent is in part contributed by the east/west circulations of the northern summer (Figs. 2.8 and 2.10), which would account for the intensity of the subtropical high during the northern summer. The equatorial trough (low pressure belt near the Equator) is found as far as 20°N during the summer monsoon season over the Asiatic land mass. The tropical pressure field has frequently been described in the meteorological literature. It should, of course, be said that the various references show some differences in the distribution of pressure for the same month in different years. The zonal asymmetries of the pressure field are consistent with the asymmetries of the other time-averaged fields discussed in the previous sections.

2.8   Precipitation Field

Here we shall present the seasonal rainfall climatology for the Tropics (40°S–40°N). This is based on TRMM (Tropical Rainfall Measurement Mission), a NASA satellite program. The use of satellite data is necessary since large parts of

the tropics are covered by oceans where there are no rain gauge- or radar-based estimates of rainfall. The TRMM-based seasonal rainfall climatology is illustrated in Fig. 2.11a–d (Zipser et al. 2006). Here the units are inches per season. This estimate of precipitation comes from microwave radiometers that are carried by the TRMM satellite. The TRMM satellite carries microwave radiation-receiving channels that are located at the following frequencies: 10.65, 19.35, 37.0, 85.5 GHz dual polarization, 22.235 GHz vertical polarization.

For completion of such analyses, data from another suite of satellites, called the US Airforce DMSP (Defense Meteorology Satellite Program), is also added to the TRMM data base. These DMSP satellites carry microwave instruments (SSM-I, special sensor microwave instrument). There are normally four such DMSP satellites available at any one time. Thus TRMM together with DMSP provide coverage from a total of five satellites that measure microwave radiances at a number of frequencies. In order to translate the microwave radiances to rainfall rates, ground truth estimates of rainfall from rain gauge and radar are required. Such ground truth data are available in many land areas, and with a particularly high density in highly-populated places such as Japan, United States, Brazil and China. It is possible to use simple multiple regression techniques to relate these directly observed estimates of rain (from rain gauges and radar) to the brightness temperatures derived from microwave radiances measured at the different channels. Under assumptions of linear dependence between the brightness temperatures TB_i at the ith channel and the rainfall R, the regression equation has the form $R = a_0 + \sum_{i=1}^{N} a_i TB_i$. If a more realistic non-linear relationship is assumed, the regression relationship is usually sought in the form $R = \exp\left(a_0 + \sum_{i=1}^{N} a_i TB_i\right) - c$ (Berg et al. 1998). Here the left hand side denotes the observed rain and the right hand side carries a number of terms each denoting a microwave channel. The multipliers a_i are the regression coefficients that are determined by a least square minimization technique. The reason this type of procedure works is that the microwave radiances which determine the corresponding brightness temperatures are emitted by the hydrometeors of the precipitating clouds. The cloud water, rain water, snow, ice and graupel all contribute to the radiances at different wavelengths. The regression procedure statistically infers the most likely rainfall rates corresponding to a given set of brightness temperatures. It must be also noted that a large sampling problem exists here. A cumulonimbus slowly passing over a rain gauge site may result in an inch of rain. A satellite, on the other hand, passes over that cloud in less than a second and cannot see all that the rain gauge does. However the premise is that over a season enough satellite passages may see a seasonal mean that may be close enough to what the rain gauge sees. Furthermore, the statistical regression is meant to push the satellite estimate of rain towards the observed estimates. Generally, the error in climatology over target areas is of the order of 15 %.
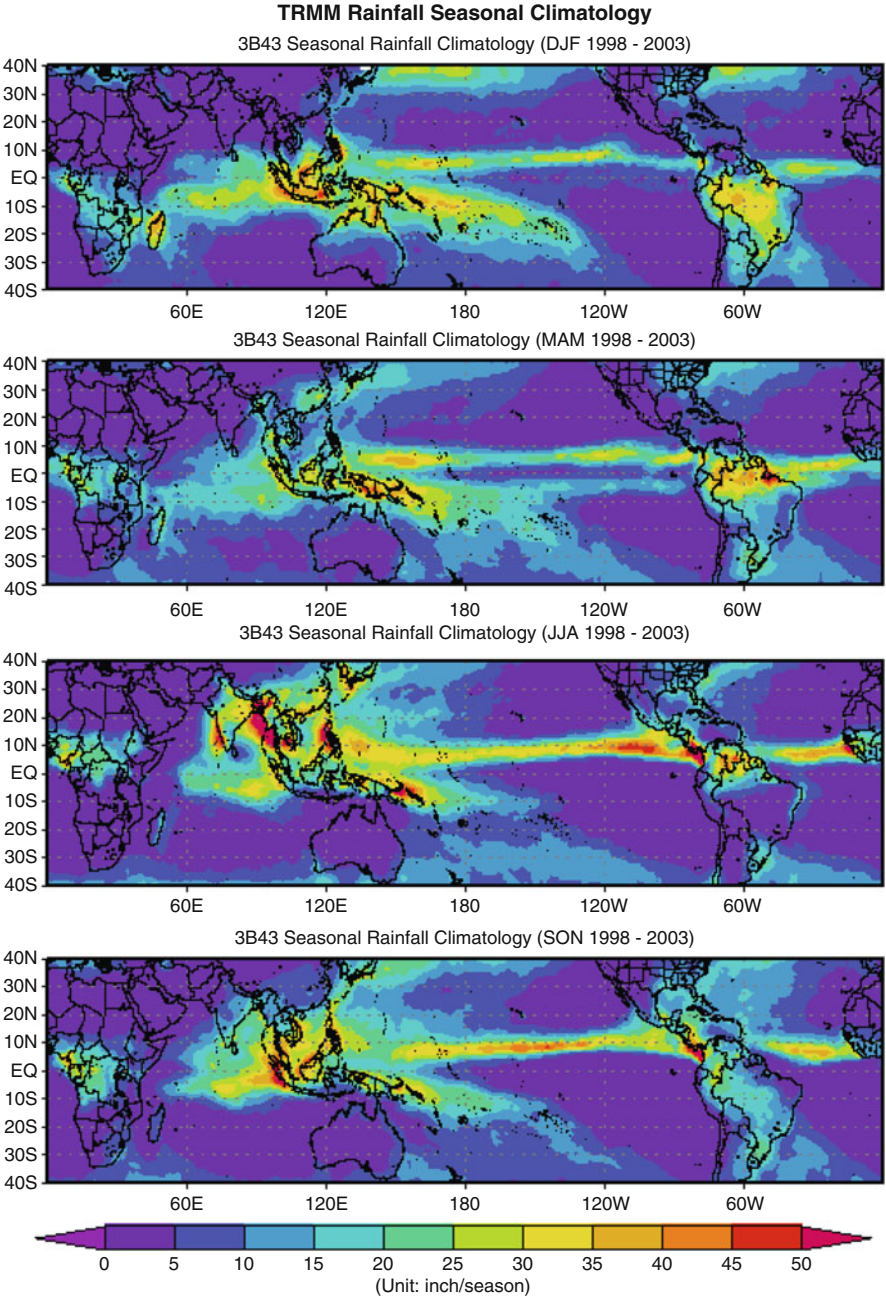
Fig. 2.11 The seasonal rainfall climatology from Tropical Rainfall Measuring Mission (TRMM) (Obtained from NASA)

The salient features seen in Fig. 2.11a–d are the following:

(i)   The ITCZ over the Pacific Ocean is very well defined by a rainfall maximum. Those maximum rainfall amounts are on the order of 50 in./season.

(ii)   The ITCZ rainfall maximum stays north of the equator over the Pacific and Atlantic Ocean near 5°–7°N over all seasons.

(iii)   A double ITCZ in the Pacific Ocean during the spring season (March, April, and May) can be noted. This includes a second belt of weaker rains 10–15 in./season near 5°S latitude over the Pacific Ocean.

(iv)   The Pacific Ocean also carries a climatological rainfall feature called the South Pacific Convergence Zone (SPCZ). This feature starts at the Western Pacific near New Guinea and slants south-eastwards towards 120°W and 40°S. This feature is known to contain a considerable amounts of non convective rain whereas the ITCZ is known to contain much larger proportions of convective rain.

(v)   Over the Indian Ocean the northern winter season sees a rainfall maximum near 5°–7°S. The heaviest northern winter rains are over Northern Australia, Southern Indonesia, Borneo, and New Guinea. The maximum rainfall is of the order of 50–100 in./season. In general, satellite estimates do not resolve extreme rainfall very well. Rain gauge estimates of heavy seasonal rainfall during northern winter can be as large as 150 in./season. This implies a roughly 50 % underestimate of the rainfall climatology by satellite estimates.

(vi)   The most interesting feature of the tropical rainfall climatology is the annual march of heavy rains from Southern Indonesia in northern winter to the eastern foothills of the Himalayas in northern summer and a reverse traverse of this rainfall belt over the rest of the year. Along this line maximum monsoon rain of 100–300 in./season of rain progress north and south during most years. This axis of heavy rains is also called the Principal Axis of the Monsoon. This rainfall belt moves to Malaysia and Myanmar in the northern spring season towards the eastern foothills of the Himalayas by the months of July and August. The retreat brings fall season rains over Southern Malaysia and Northern Borneo. This cycle is completed by January.

(vii)   Other prominent features are the summer monsoon rains over large areas of India, Indochina, and China. Over China this belt of rain goes as far North as 35°N by August. There is a considerable interannual variability of seasonal rain. Those are best seen through monthly mean data sets over several years.

(viii) The seasonal northward/southward march of rainfall is also a prominent feature over Africa. This migration from roughly 10°S in northern winter to roughly 10°N during northern summer can be clearly seen in this illustration.

(ix)   Other prominent features of the seasonal rainfall worth noting are the three main land area centers of rainfall over Borneo, Congo, and Brazil during the northern winter season.

(x)   Tropical rainfall exhibits large orographic maxima. Those are prominently seen over the Burmese Mountains in the northern spring season. Over the west coast of India during the northern summer season seasonal heavy rains are encountered along the Western Ghats.

(xi) Winter season rains, especially during November and December, over south
       eastern India arise from the fetch of northeasterly monsoon surface winds
       accumulating moisture over the Bay of Bengal.
(xii) Most tropical islands, such as Taiwan, Hawaii, Sri Lanka, Jamaica, Cuba,
       Madagascar, Borneo, Haiti-Dominican Republic and Puerto Rico exhibit
       seasonal rainfall maxima from an interaction of the tropical surface winds
       with local orography.

2.9 Other Parameters

The tropical climatologist should have a ready source of reference on the zonal
asymmetries of several other observed and derived variables that cannot be easily
presented in this kind of text. Among these, one of the most important fields is that
of sea-surface temperature. One of the best sources of reference on this is a data set
compiled by the Rand Corporation in Santa Monica, California (Alexander and
Mobley 1974). This compilation contains a global ocean temperature distribution
for a one degree latitude by one degree longitude mesh of grid points. Values of
monthly averages for all 12 months are available. The following is a list of some
other useful parameters:

(i)   Height of base and of the top of the trade wind inversion (Riehl 1945;
        Neiburger and Chien 1957)
(ii)   Monthly mean cloud amounts (Sadler 1970)
(iii) Satellite digital cloud brightness charts (Taylor and Winston 1968)
(iv)   Orography, mountain heights (Gates 1973)
(v)   Albedo of the Earth's surface (Katayama 1967a)
(vi)   Tropical monthly rainfall (Wernstedt 1972)
(vii) Monthly mean total solar radiation reaching the Earth's surface (Katayama
        1966, 1967a, b)
(viii) Net outgoing longwave radiation (Winston 1967)
(ix)   Monthly mean net solar radiation absorbed by the troposphere (Katayama
        1966, 1967a, b)

There are, furthermore, charts of dynamical parameters such as energy, momen-
tum, and moisture transports and fields of convergence of fluxes, etc. These again
exhibit large zonal asymmetries in the tropical atmosphere. We shall refer to these
in the discussions of transient motions of the atmosphere.

References

Alexander, R.C., Mobley, R.L.: Monthly average sea surface temperature and ice pack limits on a
    1 degree global grid. Rand Corporation Report, Santa Monica, pp. 1–30 (1974)

Berg, W., Olson, W., Ferraro, R., Goodman, S.J., LaFontaine, F.J.: An assessment of the first- and second-generation navy operational precipitation retrieval algorithms. J. Atmos. Sci. **55**, 1558–1575 (1998)

Flohn, H.: Contributions to a meteorology of the Tibetan Highlands. Rept. No. 130, Colorado State University, Fort Collins, 120pp (1968)

Gates, W.L.: Analysis of the mean forcing fields simulated by the two-level, Mintz-Arakawa atmospheric model. Mon. Weather Rev. **101**, 412–425 (1973)

Katayama, A.: On the radiation budget of the troposphere over the northern hemisphere (I). J. Meteor. Soc. Jpn. **44**, 381–401 (1966)

Katayama, A.: On the radiation budget of the troposphere over the northern hemisphere (II). J. Meteor. Soc. Jpn. **45**, 1–25 (1967a)

Katayama, A.: On the radiation budget of the troposphere over the northern hemisphere (III). J. Meteor. Soc. Jpn. **45**, 26–39 (1967b)

Krishnamurti, T.N.: The subtropical jet stream of winter. J. Meteor. **18**, 172–191 (1961)

Krishnamurti, T.N., et al.: 200 millibar wind field June, July, August 1967 by T.N. Krishnamurti, Edward B. Rodgers, Series: Report, Department of Meteorology, Florida State University, No. 70-2, 130 pp (1970)

Krishnamurti, T.N.: Tropical east–west circulations during the northern summer. J. Atmos. Sci. **28**, 1342–1347 (1971a)

Krishnamurti, T.N.: Observational study of the tropical upper tropospheric motion field during the northern hemisphere summer. J. Appl. Meteor. **10**, 1066–1096 (1971b)

Krishnamurti, T.N., Kanamitsu, M., Koss, W.J., Lee, J.D.: Tropical east–west circulations during the northern winter. J. Atmos. Sci. **30**, 780–787 (1973)

Krishnamurti, T.N.: Lectures on tropical meteorology in the dynamics of the tropical atmosphere. Published as colloquium notes. NCAR, Boulder, 105pp (1974)

Krishnamurti, T.N., Astling, E., Kanamitsu, M.: 200mb wind field June, July, August 1972: Atlas published by Department of Meteorology, Florida State University, Tallahassee, Florida (1975). 116p

Neiburger, M., Chien, D.: The inversion of the North Pacific Ocean Tech. Rept. No. 1, Dept. of Meteorology, University of California, Los Angeles, 74pp (1957)

Rielh, H.: Tropical meteorology. McGraw-Hill Book company, New York, 392pp (1945)

Rodwell, M.J., Hoskins, B.J.: Subtropical anticyclones and summer monsoon. J. Climate **14**, 3192–3211 (2001)

Sadler, J.C.: The feasibility of global tropical analysis. Bull. Amer. Meteor. Soc. **46**, 118–130 (1965)

Sadler, J.C.: Mean Cloudiness and gradient level wind chart over the tropics. Air weather services technical report 215, Vol. II, 60 pp (1970)

Taylor, V.R., Winston, J.S.: Monthly and seasonal mean global charts of brightness from ESSA 3 and ESSA 5 digitized pictures, February 1967–1968. ESSA Technical report NESC 46, National Environmental Satellite Center, Washington DC, 9pp, and 17 charts (1968)

Wernstedt, F.L.: World Climatic Data. Climatic Data Press, Lemont (1972). 523pp

Winston, J.S.: Planetary-scale characteristics of monthly mean long-wave radiation and albedo and some year-to-year variations. Mon. Weather Rev. **95**, 235–256 (1967)

Zipser, E.J., Cecil, D.J., Liu, C., Nesbitt, S.W., Yorty, D.P.: Where are the most intense thunderstorms on earth? Bull. Am. Meteor. Soc. **87**, 1057–1071 (2006)